2006

MCD and magnetization studies on nifB/nifZ minus molybdenum iron protein from Azotobacter vinelandii

Marcia S. Cotton
Louisiana State University and Agricultural and Mechanical College, mcotto3@lsu.edu

MCD AND MAGNETIZATION STUDIES OF *NIFB*/*NIFZ* MINUS MOLYBDENUM IRON PROTEIN FROM *AZOTOBACTER VINELANDII*

A Thesis

Submitted to the Graduate Faculty of the
Louisiana State University and
Agricultural and Mechanical College
in partial fulfillment of the
requirements for the degree of
Master of Science

in

The Department of Chemistry

by
Marcia S. Cotton
B.S., Mississippi University for Women, 1995

TABLE OF CONTENTS

LIST OF REACTIONS iv

LIST OF FIGURES v

LIST OF SCHEMES vi

ABBREVIATIONS vii

ABSTRACT ix

INTRODUCTION 1

REVIEW OF LITERATURE 3
- **Nitrogenase** 3
- **Molybdenum Nitrogenase** 4
  - **The Fe Protein** 4
  - **The MoFe Protein** 6
    - **Iron-Molybdenum Cofactor (FeMo-co)** 7
    - **P-cluster** 7
- **Electron Transfer** 9
- **Lowe-Thorneley MoFe Protein Cycle** 10
- **Maturation of MoFe Protein** 12
- **Nitrogen Fixation Genes** 13
- **Mutant Strains from *A. vinelandii*** 14
  - **Δ*nifH* MoFe Protein** 14
  - **Δ*nifB* MoFe Protein** 15
  - **Δ*nifZ* MoFe Protein** 16
  - **Δ*nifB*Δ*nifZ* MoFe Protein** 16

MATERIALS AND METHODS 18
- **Cell Growth** 18
- **Cell Lysis By Osmotic Rupture and Sonication** 18
- **Wild-Type *A. vinelandii* MoFe Protein Purification** 19
- **His-tagged *A. vinelandii* MoFe Protein Purification** 20
- **Nitrogenase Activity Assay** 21
- **Electron Paramagnetic Resonance Spectroscopy** 21
- **Magnetic Circular Dichroism Spectroscopy** 23
- **Magnetization Curves** 24

RESULTS AND DISCUSSION 25

SUMMARY AND CONCLUSIONS 33

REFERENCES 35

VITA..... 40

LIST OF REACTIONS

1. Haber-Bosch Reaction……..……. 1

2. Nitrogenase Reaction……..……4

LIST OF FIGURES

1. *A. vinelandii* nitrogenase MoFe protein structure……..…...8

2. FeMo cofactor structure……...…….8

3. P-cluster structure…….……10

4. VT-MCD spectra of Δ*nifH* MoFe protein…….……25

5. Magnetization curve of Δ*nifH* MoFe protein……..…...26

6. Magnetization curve of Δ*nifB* MoFe protein…….……27

7. VT-MCD spectra of Δ*nifB*Δ*nifZ* MoFe protein…….…29

8. Magnetization curve of Δ*nifB*Δ*nifZ* protein……...30

9. Low-temperature/High-field MCD spectra of MoFe proteins……...30

10. Experimental magnetization curves of as-isolated MoFe protein……..32

LIST OF SCHEMES

1. Fe Protein Cycle……...…….……..6

2. Electron Transfer Pathway of Nitrogenase……11

3. Lowe-Thorneley MoFe Protein Cycle……...12

4. Proposed Maturation of MoFe Protein…….…….13

ABBREVIATIONS

Å	Angstrom(s)
ADP	Adenosine 5' diphosphate
atm	Atmosphere(s)
ATP	Adenosine 5' triphophate
apo-MoFe	molybdenum iron protein with any metal-sulfur clusters absent
Av	*Azotobacter vinelandii*
β	Bohr magneton
B	Magnetic field strength
CD	Circular dichroism spectroscopy
Da	Dalton(s)
DEAE	Diethylaminoethyl
EPR	Electron paramagnetic resonance spectroscopy
E	Representative one-half tetramer of molybdenum iron protein
ε	Molar extinction coefficient
FeMo-co	Iron molybdenum cofactor
GC	Gas chromatography
g-factor	Spectroscopic splitting constant
IDS	Indigo disulfonate
IMAC	Immobilized metal-affinity chromatography
K	Kelvin
k	Boltzmann constant
MCD	Magnetic circular dichroism spectroscopy

MgADP	Magnesium adenosine 5' diphosphate
MgATP	Magnesium adenosine 5' triphosphate
nif	Nitrogen fixation gene
P cluster	[8Fe-7S] cluster of the molybdenum-iron protein
P^N	P cluster in the as-isolated, dithionite-reduced all-ferrous state
P^+	One-electron oxidized state of the P cluster relative to the P^N state
P^{OX}	Two-electron oxidized state of the P cluster relative to the P^N state
S	Electron paramagnetic spin state
T	Tesla
Tris-HCl	Tris (hydroxymethyl) aminomethane hydrochloride
VT-MCD	Variable-temperature magnetic circular dichroism
XAS	X-ray absorption spectroscopy

ABSTRACT

This study reports a characterization of the iron-sulfur clusters of the MoFe protein expressed by the *nifBnifZ* deletion strain of *A. vinelandii*. VT-MCD spectroscopic and magnetization analysis of as-isolated Δ*nifB*Δ*nifZ* MoFe protein were undertaken. VT-MCD spectra of as-isolated Δ*nifB*Δ*nifZ* MoFe protein contains bands remarkably similar to those seen in as-isolated Δ*nifH* MoFe protein, assigned to arise from an $[4Fe\text{-}4S]^{+}$ cluster. The low-temperature magnetization curve of as-isolated Δ*nifB*Δ*nifZ* MoFe protein reveals the MCD spectra bands stem from an $S = ½$ spin system with diamagnetic contributions of some other species. As-isolated Δ*nifB*Δ*nifZ* MoFe protein is compared with as-isolated Δ*nifH* MoFe protein, which contains a P-cluster precursor, and the as-isolated Δ*nifB* MoFe protein, which contains a fully assembled P-cluster ([8Fe-7S)]. Using nonlinear regression, the experimental magnetization curve of as-isolated Δ*nifB*Δ*nifZ* MoFe protein is compared and factored to contributions from as-isolated Δ*nifH* MoFe protein and as-isolated Δ*nifB* MoFe protein. The simulation suggests a 1:1 ratio of Δ*nifH* MoFe protein to Δ*nifB* MoFe protein. These results suggests the as-isolated Δ*nifB*Δ*nifZ* MoFe protein has an αβ subunit pair that contains a P-cluster and the other αβ subunit pair contains a latent (defined as immature, or potential) P-cluster (two [4Fe-4S] or P-cluster precursor).

INTRODUCTION

Nitrogen fixation, nitrification, and denitrification are three components of the geochemical Nitrogen Cycle that interconvert atmospheric dinitrogen (N_2) gas to ammonia (NH_3), nitrate (NO_3^-) ions then back into N_2 gas to complete the cycle. Since nitrogen is required for protein, amino acid, and nucleic acid synthesis, the Nitrogen Cycle is essential for all living organisms. Although dinitrogen gas is plentiful making up close to eighty percent of the atmosphere, it is a strong and stable molecule that is not easily separated. Plants and animals require N_2 to be "fixed" or converted to a useable form such as nitrates and ammonia. The phase of the Nitrogen Cycle that reduces N_2 gas into ammonia is known as Nitrogen Fixation. Nitrification converts the ammonia into nitrate ions which are returned to the atmosphere as gaseous oxides and N_2 via the denitrification process. This global cycling of nitrogen creates a continuous need of "fixed" N_2 in order to preserve every living organism.

Nitrogen fixation occurs in three different categories: (i) atmospheric, (ii) industrial, and (iii) biological fixation. Atmospheric fixation accounts for about 10 percent of the overall yield of fixed dinitrogen annually through lightning, atmospheric pollution, and combustion. Industrial fixation contributes nearly twenty-five percent of fixed N_2 via the Haber-Bosch process. The Haber-Bosch process (Reaction 1) converts N_2 and H_2 gas to NH_3 at high pressure (~200 atm) and temperature (~500 °C) over an iron catalyst.

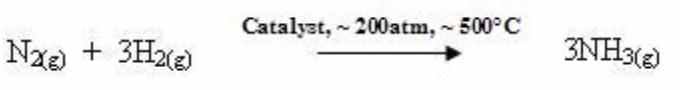

Reaction 1
Haber-Bosch Reaction

Biological fixation, occurring only in prokaryotes, is the most predominant and effective means of fixing dinitrogen accounting for sixty-five percent of fixed N_2 each year. [1, 2] 'Diazotrophs' are any biological system whether a free-living organism, in symbiotic association, or in associative symbioses capable of fixing dinitrogen at atmospheric temperatures and pressures. The variety diazotrophs range from primal bacterium (i.e., *Clostridium*) to complex legume root nodule symbioses (i.e., *Rhizobia*)

REVIEW OF LITERATURE

Nitrogenase

Nitrogenase is the catalytic system contained in diazotrophs that fixes atmospheric dinitrogen to a useable form. [3] Despite the diverse group of diazotrophs, the nitrogenase enzyme composition is quite consistent. Nitrogenase is comprised of two catalytic partner proteins called component protein 1 and component protein 2, neither of which will reduce any substrate in the absence of the other. The component proteins are numbered based on their elution from an ion exchange column. Nomenclature of the two component proteins may also refer to its bacteria source, metal content, or bacterial source in combination with elution sequence. The bacterial source nomenclature is provided using the capitalized initial of the species and the lower case initial of the genus. [4] For example, the abbreviation of Av is used to identify the nitrogenase component from *Azotobacter vinelandii*.

Metal content nomenclature of nitrogenase is based on the component protein's metal content. Component protein 2 is also known as the (iron) Fe protein because it contains a single [4Fe-4S] metal cluster. Component protein 1 varies in its metal content. The most frequently occurring nitrogenase component protein 1 contains molybdenum (Mo) and Fe thus is often referred to as the MoFe protein. When *A. vinelandii* is starved of Mo, alternate forms of nitrogenase component protein 1 arise as vanadium-iron (VFe) protein [5] and a FeFe protein is formed if both Mo and V are not present. Bacterial source in combination with elution sequence nomenclature is repeatedly used in this study as the protein components isolated from *Azotobacter vinelandii* are listed as Av1 (MoFe protein) and Av2 (Fe protein).

Molybdenum Nitrogenase

Molybdenum nitrogenase is composed of two component proteins: the Fe protein, an α_2 dimer related by a molecular two-fold rotation axis about a [4Fe-4S] cluster [6], and the MoFe protein, an $\alpha_2\beta_2$ tetramer with each αβ-dimer containing an active site iron-molybdenum cofactor (FeMoco) and a [8Fe-7S] P-cluster. [7, 8] The structural, mechanistic, functional, and maturation studies of molybdenum nitrogenase are progressing rapidly due to the determination of both the Fe protein and the MoFe protein crystallographic structures for the enzyme from *A. vinelandii*. [4, 6, 7] Atmospheric dinitrogen is reduced via an eight-electron transfer in conjunction with MgATP hydrolysis and hydrogen evolution. The molybdenum nitrogenase catalyzed reaction is shown stoichiometrically as Reaction 2.

$$N_2 + 8H^+ + 8e^- + 16MgATP \rightarrow 2NH_3 + H_2 + 16MgADP + 16P_i$$

Reaction 2
Nitrogenase Reaction

The Fe Protein

The Fe protein is 64,000 Da with two identical subunits hinged by a single [4Fe-4S]. Each subunit contains a binding site for the nucleotides, magnesium adenosine triphosphate (MgATP), and magnesium adenosine diphosphate (MgADP). [9-11]

The Fe protein's [4Fe-4S] cluster undergoes a one-electron redox cycle involving the $[4Fe\text{-}4S]^{2+}$ ($S = 0$) state and the $[4Fe\text{-}4S]^{1+}$ state. *In vivo* the Fe protein is reduced via ferrodoxin or flavodoxin, whereas *in vitro* sodium dithionite ($Na_2S_2O_4$) is used as a reductant of the Fe protein. Excess dithionite reduces the [4Fe-4S] cluster to a +1

oxidation state. The $[4Fe\text{-}4S]^{1+}$ cluster exists as a mixture of $S = 1/2$ and $S = 3/2$ spin states, where the relative amount of each state is solvent dependent. [12] The [4Fe-4S] cluster can be reduced to an all ferrous $[4Fe\text{-}4S]^{0}$ state ($S = 4$) by titanium (III) citrate (Ti(III) citrate), methylviologen, and flavodoxin but its physiological relevance is still under review. [13, 14] The MgATP-induced conformational change of the Fe protein is also a very important factor because no other redox-active agent is known to transfer electrons within the nitrogenase system to the MoFe protein such that dinitrogen is reduced. The complete progression of electron transfer within the nitrogenase enzyme system is discussed below following a discussion of both component proteins and their respective metal clusters.

In vitro, sodium dithionite reduces the Fe protein by one electron. The stoichiometric molybdenum nitrogenase catalyzed reaction, shown in Reaction 1, signifies that the Fe protein must be reduced by eight electrons to complete the conversion of dinitrogen to ammonia. After each one-electron reduction of the Fe protein, the Fe protein completes what is known as the Nitrogenase enzyme's Fe protein cycle. The Fe protein cycle is demonstrated in Scheme 1. The steps involved in the Fe protein cycle include the following: [9]

1. Following reduction of the Fe protein with a $[4Fe\text{-}4S]^{+}$ cluster, two moles of MgATP bind to the reduced Fe protein.
2. Upon MgATP-induced conformational change of the Fe protein, the Fe protein forms a complex with the MoFe protein.
3. The reduced Fe protein transfers an electron to the MoFe protein and the $[4Fe\text{-}4S]^{+}$ cluster is oxidized to the $[4Fe\text{-}4S]^{2+}$.

4. Coupled with electron transfer from the Fe protein to the MoFe protein, the two moles of MgATP are hydrolyzed.
5. The Fe protein dissociates from the MoFe protein (the rate determining step).
6. The two moles of MgADP are released.
7. The free reduced Fe protein is again reduced. This cycle is repeated until eight electrons have been transferred to the MoFe protein.

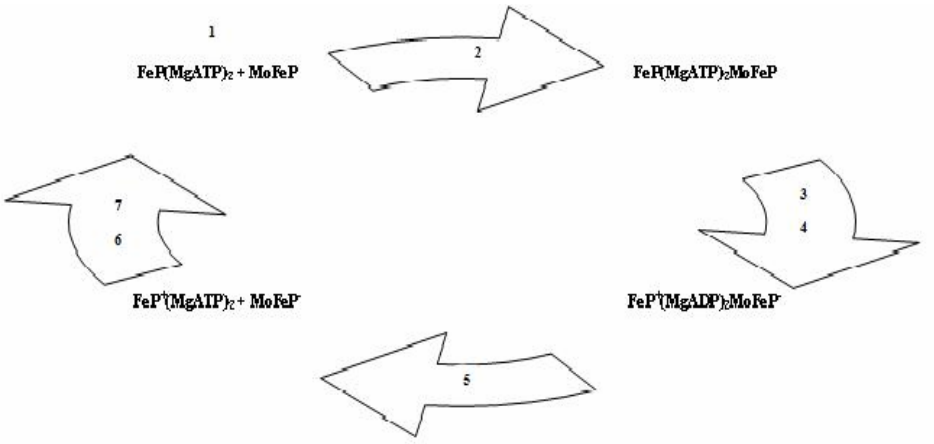

Scheme 1
Fe Protein Cycle

The MoFe Protein

The $\alpha_2\beta_2$ heterotetramer MoFe protein (Fig. 1) from *A. vinelandii* has a molecular weight of about 240,000 Da. Each αβ subunit pair contains an active site iron-molybdenum cofactor (FeMoco) and a [8Fe-7S] P-cluster and can function as a separate entity. [8] The MoFe protein metalloclusters has two main functions: (1) an electron storage and transfer and (2) substrate reduction responsibility. [9, 15]

Iron-Molybdenum Cofactor (FeMo-co)

The FeMo-co is located entirely within the α-subunit and is the site of substrate binding and reduction. As shown in Fig. 2 the cluster has a total composition [1Mo7Fe9S-X-homocitrate] assembled by a [4Fe-3S] and a [1Mo-3Fe-3S-homocitrate] cluster bridged by three inorganic sulfur atoms and shares an unknown μ_6 X atom. [7, 8, 11] The identity of the X atom is unknown, but is indicated to be a light atom (i.e. O, N, or C). [11] The FeMo cofactor is known to exist in predominantly two oxidation states with a conditional third state having been observed. In its native state, FeMoco has a distinct $S = 3/2$ EPR signal. During nitrogenase enzymatic turnover, the FeMoco is super-reduced to what is presumed be its catalytically active form ($S = 2$) which is an EPR silent state. [9] Under non-turnover conditions, the FeMoco can be chemically oxidized to produce by a third $S = 0$ state.

P-cluster

The P-cluster is interfaced between the MoFe protein's α subunit and β subunit creating an αβ subunit-pair two-fold axis. Six cysteinyl ligands (Cys-α62, α88, α154, β70, β95, and β153) coordinate the P cluster to the MoFe protein. [7] A serine ligand (Ser β188) mentioned below is relative to the P clusters oxidation state. [8] The P cluster sits about 10 Å below the MoFe protein surface [7] and is situated nearly equidistance between the [4Fe-4S] cluster of the Fe protein and the FeMoco of the MoFe protein when the Fe protein/MoFe protein complex is formed. The P-cluster accepts, stores, and transfers electrons from the Fe protein [4Fe-4S] cluster to the MoFe protein's FeMo cofactor. [15-19]

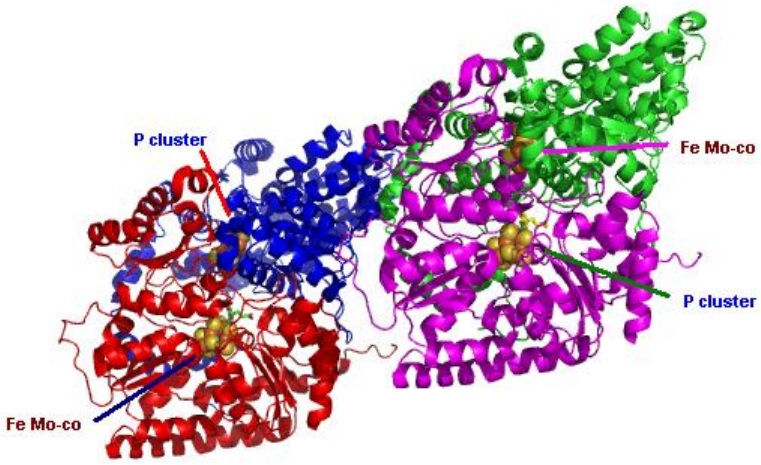

Fig. 1. *A. vinelandii* nitrogenase MoFe protein structure. (1M1N.pdb) Alpha subunits are red and green. Beta subunits are blue and purple. P-cluster and FeMo cofactor are labeled.

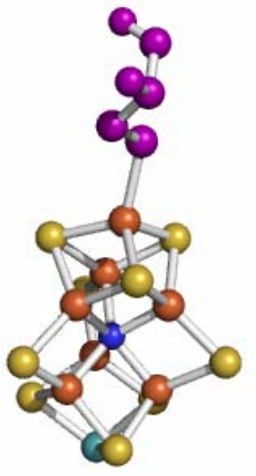

Fig. 2. FeMo cofactor structure. (1M1N.pdb). Fe atoms, sulfur atoms, and Mo atom are shown in red, yellow, and sea green, respectively. Cys-α275 and unknown atom are purple and blue, respectively.

The P cluster's X-ray crystallographic studies revealed that its structure is dependent on its oxidation state shown in Figure 3. [8] When the MoFe protein is in its reduced state, known as the native or as-isolated state, each metallocluster is labeled with the superscript of 'N' (P^N). P^N state of the P-cluster is composed of two 4Fe clusters: a [4Fe-4S] α-subunit cubane and a [4Fe-3S] β-subunit cubane bridged by an S atom. When the P cluster is two electron-equivalent oxidized, it is labeled with a superscript of 'OX' (P^{OX}). [20, 21] In the P^{OX} state, the 4Fe cubane in the β subunit is in an open conformation. The once shared S atom is now four-coordinate with three ligands from the [4Fe-3S] α-subunit cubane and one ligand from the [4Fe-3S] β-subunit cubane. The two iron atoms that were once coordinated to the shared S atom form new bonds. One coordinates with the bridging Cys-α88. The other coordinates with the aforementioned Ser-*β*188. [8]

The [8Fe-7S] P cluster has the capacity to accept and store electrons as observed by its multiple oxidation states. [15, 22] The dithionite reduced, as-isolated MoFe protein contains the P^N state of the P cluster. The P^N state of the MoFe protein, revealed by Mössbauer studies, shows all eight Fe atoms are ferrous. [22] In this native state the P cluster is EPR silent with an $S = 0$ spin state. Upon one electron equivalent oxidation of the P cluster, P^+ or $P^{SEMI\text{-}OX}$ has a mixed spin state of $S = ½$ and 5/2. [23] P^{OX} as mentioned is a two electron equivalent oxidation with an $S \geq 3$. [24]

Electron Transfer

Nitrogenase utilizes the three different metal clusters described above to transfer electrons to reduce atmospheric dinitrogen to a useable form, ammonia. Scheme 2 illustrates the trio of metal clusters and the order of electron transfer within the

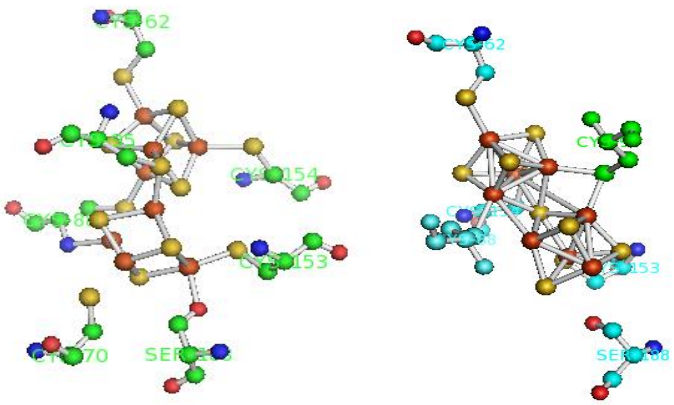

P^{OX} P^{N}

Fig. 3. P-cluster structure shown with cysteinyl ligands and oxidation state dependent structure. Iron and sulfur atoms are red and yellow. Amino acid residues are labeled.

nitrogenase. The [4Fe-4S] cluster located in the Fe protein is reduced by an external reductant. This cluster transfers an electron to the [8Fe-7S] P cluster of the MoFe protein. Electrons are then transferred from the [8Fe-7S] P cluster to the FeMo-cofactor where substrate reduction occurs. [16]

Lowe-Thorneley MoFe Protein Cycle

Turnover requires sequential delivery of single electrons from an associated Fe protein/MoFe protein complex coupled with MgATP hydrolysis followed by dissociation of the Fe protein/MoFe protein complex and the evolution of hydrogen. Representation of the overall nitrogenase mechanism is best described using the Lowe- Thorneley MoFe Protein Cycle shown as Scheme 3. As previously mentioned, the complete stoichiometric equation for dinitrogen reduction catalyzed by nitrogenase requires eight electron equivalents. Within the nitrogenase system, the Fe protein is the only known reductant of the MoFe protein that ends in conversion of dinitrogen to ammonia. Since the Fe protein systematically delivers one electron equivalent to the MoFe protein per Fe protein cycle,

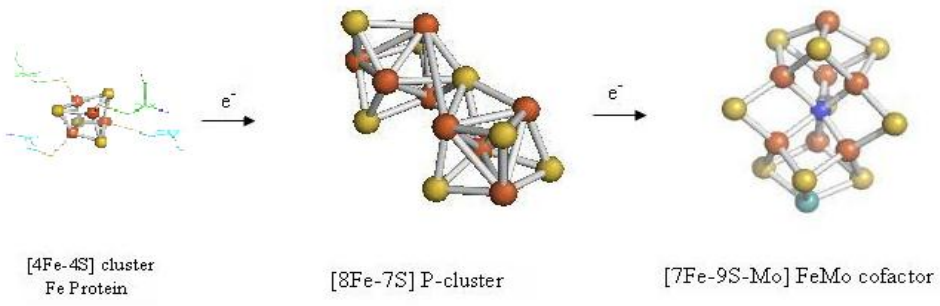

Scheme 2
Electron Transfer Pathway of Nitrogenase

the Fe protein cycle within the complete nitrogenase turnover must occur at least eight times. The Lowe-Thorneley MoFe protein cycle accounts for the sequential transfer of a single electron equivalent to the MoFe protein by way of a single Fe protein cycle. The Lowe-Thorneley MoFe protein cycle is described based on one-half of the MoFe protein represented by 'E' and is considered as one αβ subunit pair. Beginning with the dithionite reduction of 'E', the representative MoFe protein within the model, referenced as 'E_0'. The subscript number attached to 'E' refers to the number of electron equivalents provided via the Fe protein transferred following an Fe protein cycle. The Lowe-Thorneley MoFe protein cycle represents the successive transfer of eight electron equivalents from the Fe protein to the E_1, E_2, E_3, E_4, E_5, E_6, and E_7 reduced states of the MoFe protein. Stoichiometrically, nitrogenase utilizes all eight electrons although the reduction of one mole of dinitrogen requires only six electrons. The other two electrons are used in the reduction of two protons in forming one hydrogen atom. Along with the eight representative reduced states ($E_{(1-7)}$), protons and hydrogen evolution are incorporated into the Lowe-Thorneley MoFe Protein Cycle. [9, 18]

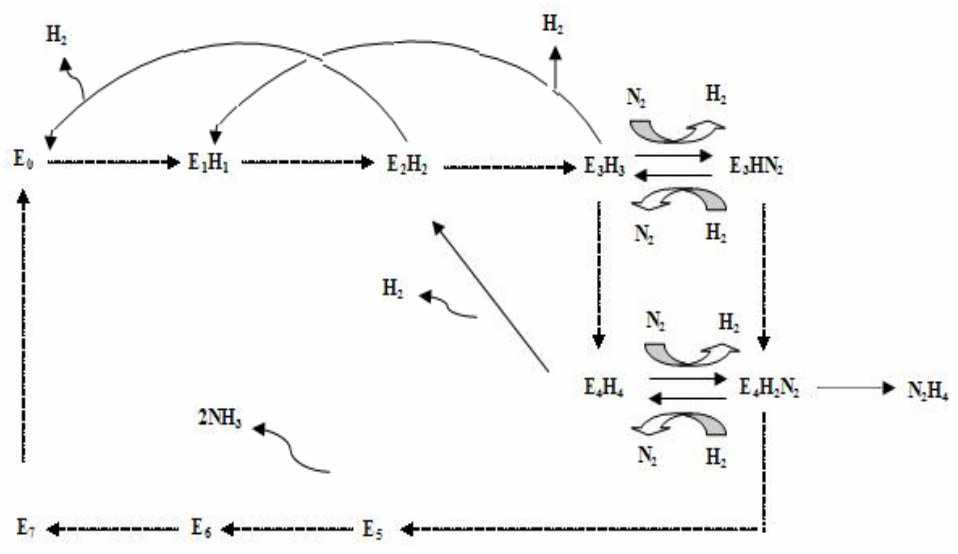

Scheme 3
Lowe-Thorneley MoFe Protein Cycle [18]

Maturation of MoFe Protein

The maturation and biosynthesis of the α subunit's FeMoco and the interfacial αβ P-cluster of the MoFe protein occurs in several steps and in separate pathways described in Scheme 4. [25] In separate pathways on its complementary scaffold, the FeMo-co is assembled and the P-cluster is assembled. [26, 27] The completely assembled FeMo cofactor is then inserted into the P-cluster containing FeMoco-deficient MoFe protein. [26] His-tagged mutant strain studies shows the MoFe protein maturates as full assembly of one half the $\alpha_2\beta_2$ tetramer before complete assembly of the second half of the $\alpha_2\beta_2$ tetramer, where the first αβ subunit contains a fully assembled P cluster and it's related α subunit contains the FeMo cofactor. The second αβ half of the tetramer subunit contains two [4Fe-4S]-like clusters located near the αβ interface with one [4Fe-4S]-like cluster in the β unit and one [4Fe-4S]-cluster in the FeMo cofactor-deficient α subunit. [Fe-S]-type

clusters are introduced onto the structured polypeptide $\alpha_2\beta_2$ tetramer. The FeMo-co site in the second αβ subunit remains unfilled until a maturated P cluster occupies the αβ interface.

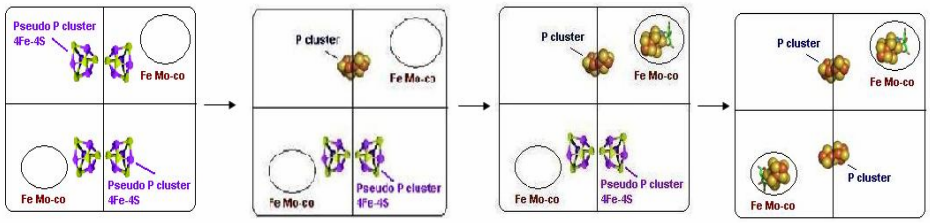

Scheme 4
Proposed Maturation of MoFe Protein

Nitrogen Fixation Genes

A plethora of genes known as **ni**trogen **f**ixation (*nif*) genes are related to the maturation and biosyntheses of nitrogenase component proteins and metalloclusters. [28] The nomenclature for genes and gene products are expressed as follows: if *nifX* is the gene then NifX is the gene product (i.e., protein) encoded by *nifX*. *nifH*, *nifD*, and *nifK* are the structural genes that encode the Fe protein, the α subunit of the MoFe protein, and the β subunit of the MoFe protein, respectfully. Although many of the *nif* genes specific to the biosynthesis of FeMo-co have been identified, to date no *nif* genes whose function is exclusively for the synthesis of the P-clusters have been identified. The notion of the biosynthetic assembly of the [8Fe-7S] P-cluster involving the fusion of two [4Fe-4S]-clusters is a reasonable postulation. [29] The current study offers and extends the characterization of three apo-MoFe proteins that aid in understanding the complexities of the metallo P-cluster.

Mutant Strains from *A. vinelandii*

Apo-protein refers to the nitrogenase protein component with any or all metal-sulfur clusters removed. [30, 31] The apo-MoFe protein occurring after the polypeptide structure is complete and before the complete assembly of one or both P-cluster and FeMo-co is representative of the proteins used in this study. The apo-MoFe proteins studied here are void its FeMo cofactor unless otherwise noted.

This study comparatively analyzes the MCD and magnetization properties of the variant P-clusters from *A. vinelandii* His-tagged mutant strain Δ*nifB*Δ*nifZ* MoFe (expressed in *Av* strain YM6A) [25] with the novel P-cluster from *A. vinelandii* His-tagged mutant strain Δ*nifB* MoFe (expressed in *Av* strain DJ1143) [31, 32] and P-cluster precursor from *A. vinelandii* His-tagged mutant strain Δ*nifH* MoFe (expressed in *Av* strain DJ1165) provided by Markus Ribbe (Department of Molecular Biology and Biochemistry, University of California Irvine). [33] Variable-Temperature Variable Field Magnetic Circular Dichroism (VTVH-MCD) Spectroscopy and Magnetization Studies are used to characterize the type and electronic properties of the Fe-S clusters of in Δ*nifB*Δ*nifZ* MoFe protein.

Δ*nifH* MoFe Protein

Biochemical and spectroscopic studies indicate the MoFe protein isolated from a *nifH*-deleted strain of *A. vinelandii* contains 2[4Fe-4S]-like clusters that most likely are the biosynthetic P cluster precursors. His-tagged Δ*nifH* MoFe protein has two [4Fe-4S]-like clusters per αβ subunit as XAS analysis predicted the latent P cluster of Δ*nifH* MoFe as a pair of [4Fe-4S]-like cluster consistent with the results shown in recent publication. [34, 35] The as-isolated Δ*nifH* MoFe protein exhibits a paramagnetic S = ½ EPR signal

arising from 2-[4Fe-4S]$^{+}$ clusters. The EPR spectrum of *nifH*-deleted strain of *A. vinelandii* reveals absence of FeMo-co typical $S = 3/2$ signal. [33] The *nifH* gene encodes the Fe protein, NifH. [28] Because the Δ*nifH* MoFe protein is very oxygen sensitive and unstable, to date the crystal structure has not been produced. The Δ*nifH* apo-MoFe protein can complex with Fe protein-$(MgATP)_2$ and carry out MgATP hydrolysis but can not reduce substrate. The Δ*nifH* apo-MoFe protein is in a compact conformation that requires the presence of Fe protein and MgATP before isolated cofactor may be inserted. [33]

Δ*nifB* MoFe Protein

Deletion of *nifB* in *A. vinelandii* results in an apo-MoFe protein that is void of FeMo cofactor. The Δ*nifB* MoFe protein may be a reflection of the last phase of the maturation of MoFe protein. [25] The *nifB* gene encodes NifB that provides a platform designated NifB-cofactor supporting the synthesis of an iron and sulfur-containing assembly forming FeMo cofactor. [31] Although Δ*nifB* MoFe protein is able to complex with Fe protein-$(MgATP)_2$ and carry out 60% of normal MgATP hydrolysis it is catalytically inactive or incapable of reducing substrates. The catalytic activity of Δ*nifB* MoFe protein can be reconstituted by direct insertion of purified FeMo cofactor into the open FeMo-co binding site. [36] The crystal structure Δ*nifB* MoFe protein shows that it is analogous to the wild-type MoFe protein except for the open FeMo-co binding site domain indicating that the FeMoco binding site in Δ*nifB* MoFe protein is readily accessible for FeMoco insertion. [28] X-ray crystallography shows that the structures of the P clusters of apo-MoFe protein isolated from a *nifB*-deletion strain of *A. vinelandii* has the same form as found in wild-type MoFe protein. XAS edge and EXAFS analysis

confirm the presence of a normal P-cluster [37] and redox-dependent structural change representing a two-electron oxidation analogous to the wild-type MoFe protein P-cluster. [19]

Δ*nifZ* MoFe Protein

Based on EPR spectroscopy, metal analysis, and activity assays the following compositions are assumed. An apo-MoFe protein isolated from a His-tagged *nifZ*-deletion strain of *A. vinelandii* is composed of one subunit pair that has one fully assembled P cluster bridged between the α and β subunit and one FeMo-co located in the α subunit. The other αβ subunit pair has a presumed latent P-cluster comprised of a pair of [4Fe-4S]-like clusters. NifZ (*nifZ* gene product) of *A. vinelandii* has been demonstrated as being required for the expression of a fully functional MoFe protein. Although characterization and purification of NifZ is still underway, it alone or in combination with other components has been proposed to have a chaperone-like fashion to facilitate a conformational rearrangement that is required for the formation of the second P cluster and the subsequent insertion of FeMoco into the vacant FeMoco binding site. [25]

Δ*nifB*Δ*nifZ* MoFe Protein

Since the deletion of the *nifB* gene results in the expression of a FeMoco-deficient form of MoFe protein, [31, 36] His-tagged Δ*nifB*Δ*nifZ* MoFe protein is presumed to have the same composition as His-tagged Δ*nifZ* MoFe protein but does not contain the FeMo-co center in either αβ dimer. Results of His-tagged Δ*nifB*Δ*nifZ* MoFe protein and His-tagged Δ*nifZ* MoFe protein studies suggest that MoFe protein is likely assembled in a

stepwise fashion, i.e. one αβ subunit pair of the tetrameric MoFe protein is assembled prior to the other. [25]

MATERIALS AND METHODS

Cell Growth

A. vinelandii were grown at Virginia Tech and University of California, Irvine. [25] Harvested cells were stored at -80C until used. All protein handling were performed under an Argon atmosphere using a Schlenk line system [38] and a Vacuum Atmospheres glove box with an oxygen level of < 3ppm. The Schlenk line system allows the independent maintenance of gas pressure and vacuum control by way of a common point using a three way stopcock. This system allows the multiple-neck round-bottom flask or vial connected to it (vacuum tubing) to be either under pressure, under vacuum, or isolated. Each buffer is degassed under Argon and contains 2mM sodium dithionite ($Na_2S_2O_4$) prior to use. Unless otherwise noted all chemicals and reagents were obtained from Sigma-Aldrich or Fisher Scientific.

Cell Lysis By Osmotic Rupture and Sonication

Between 200 and 300 g of harvested *A. vinelandii* cells were divided into 50 to 60 g aliquots and lysed by either osmotic shock or sonication. The 50 g aliquots of frozen *A. vinelandii* cells were placed into 250 ml centrifuge bottles. The rupture of *A. vinelandii* cells by osmotic shock begins with the addition of glass shards that aid in balancing the centrifuge bottles, mixing the cell suspension, and rupturing the harvested cells. The cells were allowed to thaw inside glove box with O_2 levels less than 1 ppm. The inner caps and screw tops were tightened before removing the thawed cells from the glove box. The thawed cells were immediately placed on ice. While allowing a flow of Argon gas into each centrifuge bottle, the cells were suspended in 4 M glycerol in 0.025 M Tris-HCl buffer at pH 8. The cell suspension was mixed by shaking each bottle and immediately

placed back on ice for about 45 minutes to allow glycerol swelling of the cells. The cells were then centrifuged at 10,000 RPM (Sorvall® Model:RC-5B with a GSA rotor) for 30 minutes at 10°C. The excess glycerol that was not taken up by the cells was decanted and over a constant flow of Argon gas and a small amount of deoxyribonuclease I (DnaseI) and 0.025 M Tris-HCl buffer, pH 8 was added to the glycerol-swollen cells. The individual bottles were shaken vigorously until cells were loosened and removed from the walls of each bottle. The glycerol-swollen cells were allowed to fully rupture by incubation in the 0.025 M Tris-HCl buffer for 10 minutes on ice. After the cells ruptured the supernatant was centrifuged at 13,000 RPM for 40-60 minutes at 4°C. The pellets were discarded and the clear-dark supernatant/crude extract was decanted into a large round bottom flask.

The use of sonication of harvested cells to obtain crude extract of cells differs from osmotic rupture in that the 4M glycerol in 0.025M Tris-HCl buffer is not introduced to the cells. After aliquots of harvested cells were placed into 250 ml centrifuge bottles, the bottles were balanced by adding 0.025M Tris-HCl buffer at pH 8. Parafilm was placed over each bottle and punctured enough to allow the probe of a Branson sonifier (Branson Sonic Power Company, Danbury, CT) and a constant flow of N_2(g). The output control was set to 8 and probe was alternated "on" for 1 ½ minutes and "off" for 30 seconds. This process was repeated a total of 10 times. The solution turned dark and was then centrifuge @ 13,000 RPM for 40 minutes at 4°C.

Wild-Type *A. vinelandii* MoFe Protein Purification

Using a Rabbit® pump at a rate between 30 to 40 ml/min, the crude extract was loaded onto an anaerobic DEAE sepharose column pre-washed with 0.025M Tris-HCl

buffer pH 8 until column was found to be reducing. The loaded crude extract was subjected to a linear gradient of 0.025M Tris-HCl pH 8 buffer to 1M NaCl/0.025M Tris-HCl pH 8 buffer. The *A. vinelandii* nitrogenase protein components are separated, eluted, and collected in fractions. The MoFe protein (Av1) eluted between 0.20 M and 0.25 M NaCl. The Fe protein (Av2) eluted between 0.30 M and 0.35 M NaCl.

The MoFe protein from the crude separation was further purified by applying a linear gradient of NaCl on a Q-sepharose column applying same buffer solutions as previously mentioned.

His-tagged *A. vinelandii* MoFe Protein Purification

The mutant strains expressing His-tagged protein were purified using a convenient IMAC, Immobilize Metal Affinity Chromatography system (Amersham Pharmacia). The IMAC column was washed with 3 to 4 bed volumes of charged buffer (400mM Zn - $7H_2O$ solution and equilibrated with 250 ml of 0.5M NaCl/ 20mM Tris-HCl, pH 7.9). The crude extract as previously described but now containing a poly-His tagged MoFe (Av1) was loaded onto the column at a rate of 10 ml/min. Poly-His tagged MoFe (Av1) shows a strong binding affinity to the immobilized Zn(II)-ions, whereas protein (Fe protein) showing nearly no interaction for the Zn(II)-ions eluted immediately. Next the column was washed with 2 to 3 bed volumes of binding buffer (20mM Imidazole/0.5M NaCl/20mM Tris-HCl pH 7.9) until eluting solution became white. Poly-His tagged MoFe protein was eluted after applying about 80 ml of 250mM Imidazole/0.5M NaCl/20mM Tris-HCl pH 7.9 buffer to column. The eluted His-tagged MoFe protein was collected directly into an anaerobic 3-neck flask.

Nitrogenase Activity Assay

Hydrogen evolution assay was used to monitor protein activity. A rubber-stoppered 13.8 ml glass vial served as the reaction vessel. The reaction vessels are vacuumed and filled with Argon gas using a schlenk manifold. This process is repeated for each vessel (2 X 3 minutes) for vacuum and filled with Argon gas. Hamilton Gas Tight® syringes are used for any transfer into reaction vessel. Each Ar-filled reaction vessel contained 1 ml of ATP-regenerating solution and 20 mM sodium dithionite ($Na_2S_2O_4$) solution. 20 mM sodium dithionite solution was obtained by neutralization of $Na_2S_2O_4$ with 0.25 M NaOH. ATP-regenerating solution contained 5 mM $MgCl_2$-$6H_2O$, 0.125 $mgml^{-1}$ creatine phosphokinase, 38 mM TES-KOH (pH 7.4), 2.5 mM ATP, and 30 mM phosphocreatine.

Depending on the assay desired whether for Av1 or Av2, relative amounts of component proteins of known activity were added to each reaction vial. Each reaction vial was then allowed to incubate at 30° C for ten minutes. After appropriate time 0.5 ml of headspace gas was withdrawn using a Hamilton Gas Tight® with pressure-lock syringe. The amount of hydrogen evolved was determined using a Shimadzu GC-8A equipped with an 80/100 molecular sieve 5A column (He) and a thermal conductivity detector.

Electron Paramagnetic Resonance Spectroscopy

Electron Paramagnetic Resonance (EPR) Spectroscopy is a technique that detects unpaired electrons in complexes by their resonant absorption of microwave radiation in an external magnetic field. EPR spectroscopy provides structural and environmental information, electron distribution, and sometimes the geometry of paramagnetic

molecules. The most valuable characteristic of any EPR spectrum is the constant known as the g-factor, g. The g factor of a free electron is $g_e = 2.0023$.

Since unpaired electrons are very sensitive to its environment, the g factor will deviate from g_e as a free electron's environment change. Spin-orbital coupling is the interaction of the intrinsic spin of an electron and its orbital motion. Therefore, spin-orbit coupling results in a g factor greater or less than that of g_e as the local field can either oppose or add to the applied field. In turn, the appearance of an EPR spectrum (and g factors) will vary due to the paramagnets orientation or anisotropy. Four limiting cases are listed:

1.) Isotropic paramagnet: Symbolic of a sphere reveals a single symmetric EPR absorption when orientation is not a factor. $g_x = g_y = g_z$

2) Low-field axial paramagnet: Symbolic of a football reveals a low-field minor feature (g_z) and a high-field major feature ($g_x = g_y$). $g_x = g_y < g_z$

3) High-field axial paramagnet: Symbolic of a discus reveals a high-field minor feature (g_z) and a low-field feature ($g_x = g_y$). $g_x = g_y > g_z$

4) Rhombic paramagnetic: Symbolic of a semi-deflated football reveals three different values. $g_x \neq g_y \neq g_z$

Last if the paramagnet interacts with nuclei with a non-zero magnetic moment this produces a local magnetic field resulting in the splitting of a single EPR signal. This is termed hyperfine interaction.

The EPR spectra results of each apo-MoFe protein studied in this work provides further insight into the similarities and differences of the novel P-clusters and the latent P-clusters.

Magnetic Circular Dichroism Spectroscopy

Magnetic Circular Dichroism (MCD) spectroscopy probes the geometric and electronic structures of transition metal complexes of metalloproteins making it extremely useful for identifying types iron-sulfur clusters and their spin states. [39] MCD is a measurement of the differential absorption of left and right circularly polarized light induced in a magnetic field parallel to the propagation of light. All samples include fifty percent glycerol to enable the formation of optical glasses at low temperatures. The experimental quantity measured in MCD is ΔA. $\Delta A = A_L - A_R$, where A_L and A_R are absorbance in left and right circular polarized light. ΔA is related to $\Delta\varepsilon$ ($\Delta\varepsilon = \varepsilon_L - \varepsilon_R$), which is the difference between the molar extinction coefficients of left and right circularly polarized light.

Variable-Temperature Variable-Field Magnetic Circular Dichroism (VTVH-MCD) spectra were measured using a JASCO Model J-710 spectropolarimeter for the 350-800 nm region. An OXFORD Instruments Spectromag 4000-7T superconducting magnet can generate a magnetic field up to 7T. Protein sample temperatures were determined with a LAKESHORE Cryogenics Cernox Model CX1050-Cu-1-4L sensor placed above and below the sample. Temperatures below 4.22K were maintained by continuously pumping on a liquid helium bath using a rotary vane pump. Each protein sample contained 50% (v/v) glycerol as a glassing agent for low-temperature MCD studies. Frozen samples prepackaged in anaerobic 0.1 cm or 0.2 cm Starna Cells Spectrosil® Quartz cells were shipped via dry ice and immediately stored in liquid nitrogen dewars until MCD spectra were acquired. Starna Cells Spectrosil® Quartz cells are fused using only heat and no intermediate adhesives. Protein samples were placed in

the sample holder and immersed into sample chamber under a continuous flow of helium gas. Low temperature MCD spectra were obtained by taking the difference of two opposing fields (positive and negative) dividing by two. This eliminates the CD portion of the observed spectra and leaves only the MCD component. Spectra are expressed as the difference in the molar extinction coefficients, $\Delta\varepsilon$, for right and left circularly polarized light normalized per unit with units of $cm^{-1}M^{-1}$.

Magnetization Curves

Magnetization curves establish the nature of the paramagnetic species giving rise to an MCD spectrum by monitoring the saturation properties of absorption maxima bands as a function of increasing or decreasing of magnetic field or temperature. Magnetization curves may be plotted as percent magnetization versus $\beta B/2kT$, magnetic field, or $1/T$; where β is the Bohr magneton, B is the magnetic field strength, k is the Boltzmann constant, and T is the absolute temperature. Magnetization curves add information useful for resolving and assigning electronic transitions such as estimations of the ground state spin state, g-factors, and zero-field parameters. [39-41] Theoretical magnetization curves in this study were simulated using the Saturation Magnetization. 3.1.1. Simulation Program described by Frank Neese and Edward I. Solomon. [42]

The magnetization data of the His-tagged Δ*nifB* MoFe protein is corrected to 520 nm by extrapolation of MCD intensity proportional to acquired magnetization obtained at 406 nm.

RESULTS AND DISCUSSION

Dithionite-reduced and IDS-oxidized His-tagged Δ*nifH* MoFe protein [33] from *A.vinelandii* were examined by variable temperature MCD spectroscopy and magnetization studies. All signals in this study arise only from the P-cluster precursors present in Δ*nifH* MoFe protein from *A.vinelandii* due to the absence of FeMo-co. [34]

The variable temperature MCD spectra of dithionite-reduced Δ*nifH* MoFe protein shows temperature-dependent bands increasing in intensity as temperature decreases. The dithionite-reduced His-tagged Δ*nifH* MoFe protein MCD spectra shown in Fig. 4 are at temperatures 1.5K, 4.2K, and 10K. The band patterns are characteristic of synthetic and biological $S = ½$ $[4Fe\text{-}4S]^{+}$ clusters. Most notable are the multiple positive bands between 350 and 520 nm, the broad positive bands in the 700 to 800 nm region, and the negative bands centered between 600 and 700 nm. [43]

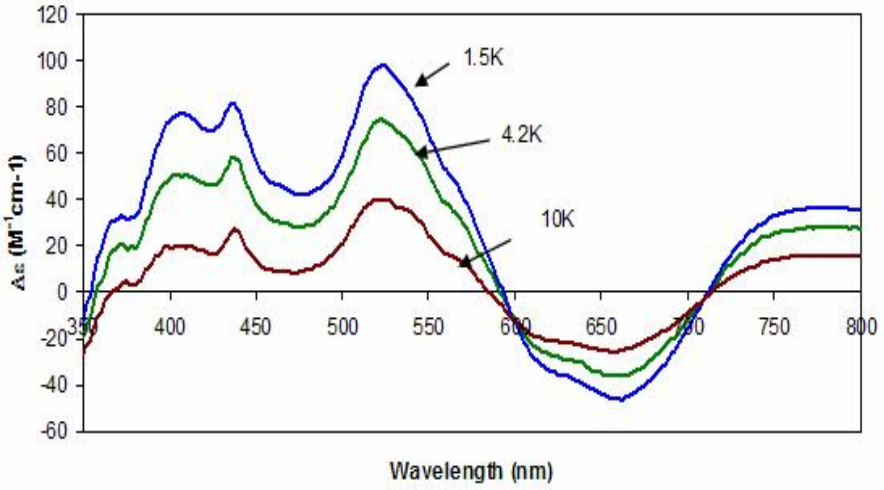

Fig. 4. VT-MCD spectra of Δ*nifH* MoFe protein. Dithionite-reduced His-tagged Δ*nifH* MoFe protein from *A. vinelandii*. Temperatures of 1.5K (blue), 4.2K (green), and 10K (red). Magnetic field of 6T.

MCD magnetization curve of dithionite-reduced Δ*nifH* MoFe protein at 1.5K shown in Fig. 5 shows a theoretical simulation of an isotropic $g = 2$ and $S = 1/2$ spin state as a solid black line. The experimental magnetization curve of dithionite-reduced Δ*nifH* MoFe protein as compared to the theoretical simulated isotropic $g = 2$ and $S = 1/2$ spin state magnetization curve are nearly identical. The small increase in the initial slope of the magnetization curve of dithionite-reduced Δ*nifH* MoFe protein is a result of the presence of an S = 5/2 spin system. [34]

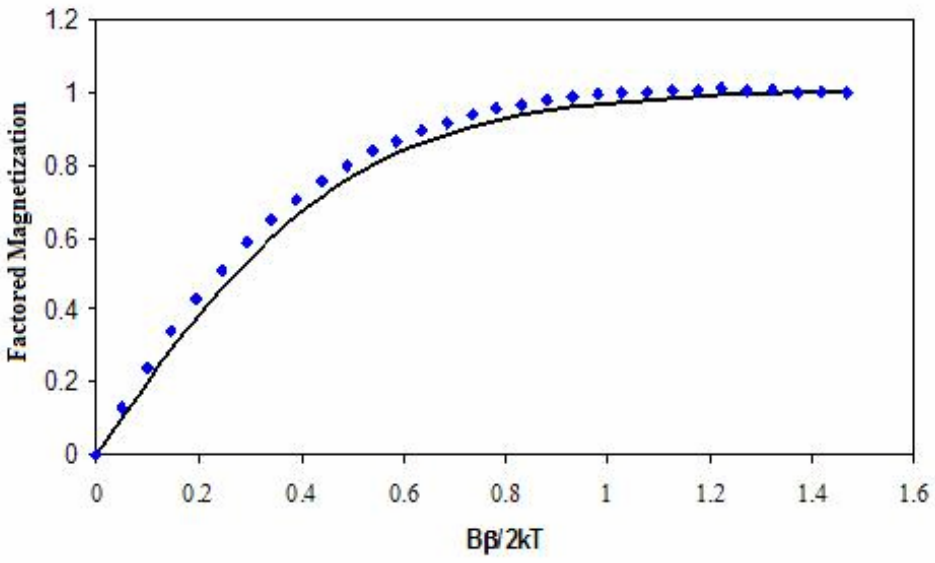

Fig. 5. Magnetization curve of Δ*nifH* MoFe protein. Dithionite-reduced His-tagged Δ*nifH* MoFe protein (blue diamond) at 520 nm. Temperature at 1.5K and magnetic field 0 to 6T. Theoretical magnetization curve (solid black) of isotropic $g = 2$, $S = ½$ spin system.

MCD spectroscopy provides a direct discrimination of paramagnetic versus diamagnetic species. [44, 45] A paramagnetic species as dithionite-reduced His-tagged Δ*nifH* MoFe protein as described above has temperature-dependent MCD spectra that increases in intensity as the temperature is lowered. This temperature dependence is due

to Boltzmann population distribution over the ground state Zeeman components. [45, 46] The MCD spectra of variable temperatures for a diamagnetic species show independence to temperature. [40]

The VT-MCD spectra of dithionite-reduced Δ*nifB* MoFe protein revealed temperature-independent signals indicative of a diamagnetic state (not shown). [34] This same diamagnetic state is recognized in the as-isolated dithionite-reduced wild-type MoFe protein from a fully assembled-EPR silent P-cluster. [15, 17, 23, 32] The EPR spectrum of the dithionite-reduced Δ*nifB* MoFe protein lacks the $S = 3/2$ signal, confirming the absence of FeMoco. [47]

The magnetization curve at 406 nm of dithionite-reduced Δ*nifB* MoFe protein shown in Fig. 6 is nearly linear and temperature independent (not shown) indicates the P-clusters are indeed diamagnetic and comparable to the P^N state of the P-cluster in the wild-type MoFe protein. [22]

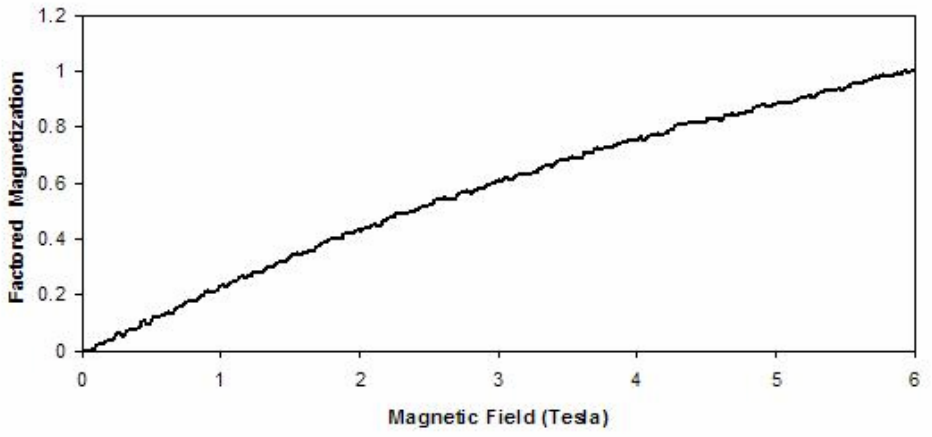

Fig. 6. Magnetization curve of Δ*nifB* MoFe protein. Dithionite-reduced His-tagged Δ*nifB* MoFe protein. T = 1.5K and 406 nm.

EPR spectroscopy studies of dithionite-reduced His-tagged Δ*nifB*Δ*nifZ* MoFe protein does not exhibit the $S = 3/2$ signal [25] indicative of the FeMoco center as seen in the wild-type MoFe protein [9] and dithionite-reduced His-tagged Δ*nifZ* MoFe protein. [25] The $g = 2$ region of dithionite-reduced His-tagged Δ*nifB*Δ*nifZ* MoFe protein EPR spectrum reveals an $S = ½$ signal [25] similar to the dithionite-reduced Δ*nifH* MoFe protein and attributable to the two [4Fe-4S]-latent P^+ cluster. [34, 36]

The presence of a $g = 11.8$ parallel mode EPR signal is ascertain to the IDS-oxidized (P^{OX}) state of the P-cluster present in both the IDS-oxidized wild-type [22, 24] and Δ*nifB* MoFe protein signal. [47] IDS oxidation of oxidation of Δ*nifB*Δ*nifZ* MoFe protein yields this $g = 11.8$ signal analogous to [25] both the IDS-oxidized wild-type and Δ*nifB* MoFe protein. The only difference between the two signals is the IDS-oxidized Δ*nifB*Δ*nifZ* MoFe protein signal integrated to about 50% the IDS-oxidized wild-type and Δ*nifB* MoFe protein signal. [25]

The MCD spectra in the 350-800 nm region of the dithionite-reduced His-tagged Δ*nifB*Δ*nifZ* MoFe protein (Fig 7) at temperatures of 1.5, 4.2, and 10K show that the bands are temperature dependent with an increase of signal intensity as temperature decreases signifying a paramagnetic active species. [40] The MCD band patterns are similar in form and intensity to the $S = ½$ $[4Fe\text{-}4S]^+$ clusters of dithionite-reduced His-tagged Δ*nifH* MoFe protein [34] with the exception of the crossover point above zero and that the negative band between 600 and 700 nm is not as prominent as in the dithionite-reduced His-tagged Δ*nifH* MoFe protein. The intensity of the low temperature MCD spectra for dithionite-reduced Δ*nifB*Δ*nifZ* MoFe protein are indicative of the presence of at least one $S = ½$ $[4Fe\text{-}4S]^+$ cluster. [43, 45] MCD magnetization data collected at 520

nm shown in Fig. 7 revealed a chromophore with an initial slope less than the slope of the theoretical magnetization curve of an isotropic $S = ½$ spin system.

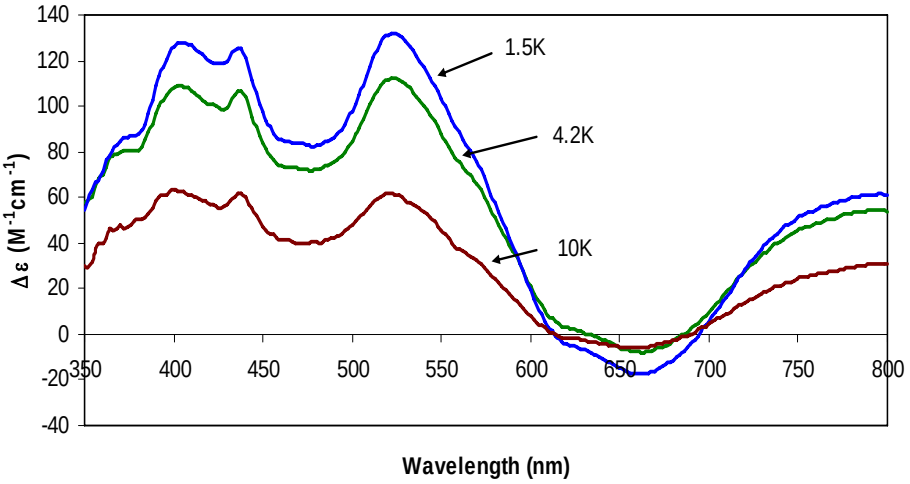

Fig. 7. VT-MCD spectra of Δ*nifB*Δ*nifZ* MoFe protein. Dithionite-reduced His-tagged Δ*nifB*Δ*nifZ* MoFe protein from *A. vinelandii*. Temperature 1.5K (blue), 4.2K (green), and 10K (red). Magnetic field of 6T.

The magnetization curve of dithionite-reduced Δ*nifB*Δ*nifZ* MoFe protein (Fig. 8) at 1.5K and 520 nm has an initial slope less than that of an isotropic $g = 2$ and $S = ½$ spin state theoretically simulated magnetization curve (solid black line in Fig. 8). The difference in initial slope intensity suggests a contribution from a species other than an S =1/2 spin system, more than likely that of a diamagnetic species.

The low-temperature/high-field MCD spectra of the as-isolated, dithionite-reduced His-tagged Δ*nifB* MoFe, Δ*nifH* MoFe, and Δ*nifB*Δ*nifZ* MoFe proteins are shown in Fig. 9. The spectra of dithionite-reduced His-tagged Δ*nifH* MoFe protein [34] and dithionite-reduced His-tagged Δ*nifB*Δ*nifZ* MoFe protein have a couple of positive bands between 350 and 520 nm, another less intense positive band at 800 nm and a negative

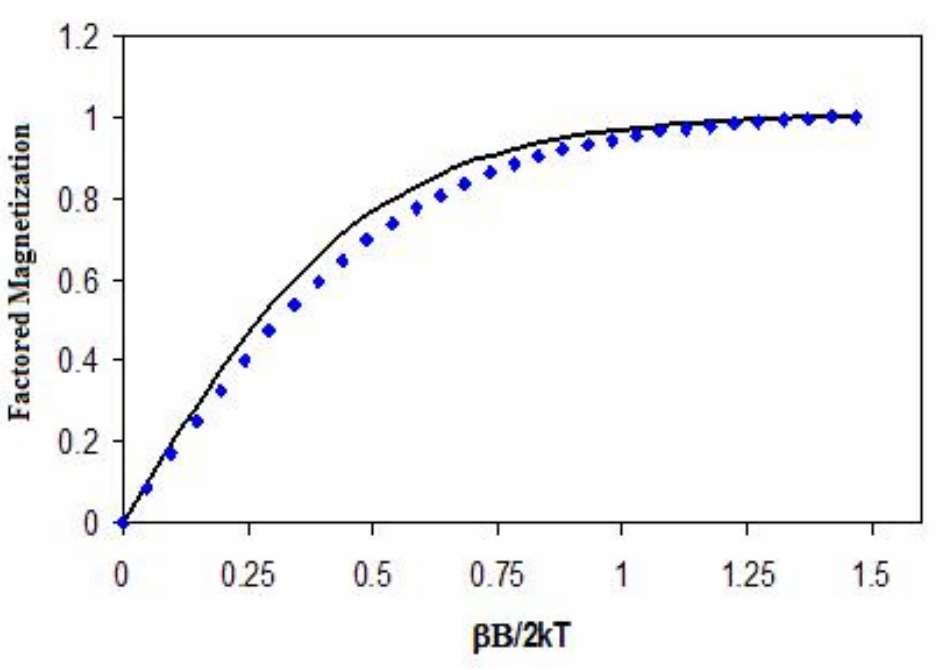

Fig. 8. Magnetization curve of Δ*nifB*Δ*nifZ* MoFe protein. Dithionite-reduced His-tagged Δ*nifB*Δ*nifZ* MoFe protein from *A. vinelandii* (blue diamonds). Theoretical magnetization curve (black) of isotropic $g = 2$ and $S = ½$ spin system.

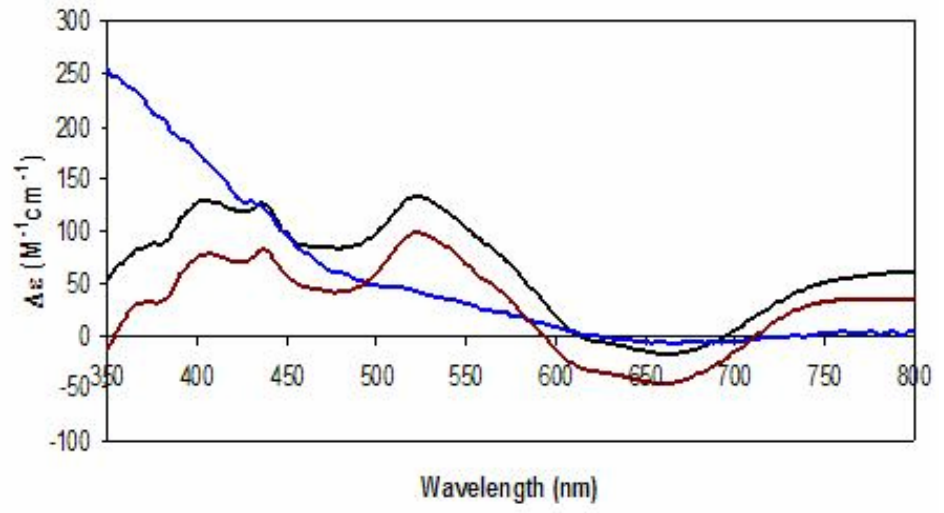

Fig. 9. Low-temperature/High-field MCD spectra of MoFe proteins. Dithionite-reduced His-tagged Δ*nifB* (blue), Δ*nifH* (red), and Δ*nifB*Δ*nifZ* (black) MoFe protein. T = 1.5K and magnetic field of 6T.

band at 680 nm that are typical of [4Fe-4S] cluster(s) in a +1 oxidation state. [39, 41, 43, 46, 48] MCD spectrum of the diamagnetic dithionite-reduced His-tagged Δ*nifB* MoFe protein remains relatively positive throughout the visible region. [34]

Observation that the magnetization curve of dithionite-reduced Δ*nifB*Δ*nifZ* MoFe protein does not consist of a pure $S = ½$ species and VTVH-MCD suggests the as-isolated, dithionite-reduced Δ*nifB*Δ*nifZ* MoFe protein contains a fully assembled P-cluster and a latent P-cluster identical to that found in the as-isolated, dithionite-reduced Δ*nifH* MoFe protein. As a result component contributions in relation to magnetization were explored. Using nonlinear regression, factored contributions from Δ*nifH* MoFe protein and Δ*nifB* MoFe protein magnetization curves are simulated and compared to the experimental magnetization curve of *nifB*Δ*nifZ* MoFe protein.

The magnetization curve of dithionite-reduced Δ*nifB* MoFe protein [34] multiplied by best fit estimation of contribution of dithionite-reduced Δ*nifB*Δ*nifZ* MoFe protein magnetization curve has a value of 1.00 (Fig. 10). The magnetization contribution at 520 nm of dithionite-reduced Δ*nifB* MoFe protein is representative of the P^N state of the P-cluster. The P^N state of the P-cluster is diamagnetic. The diamagnetic contribution of the P^N state contributes to the magnetization of dithionite-reduced Δ*nifB*Δ*nifZ* MoFe protein.

The magnetization curve of dithionite-reduced Δ*nifH* MoFe protein multiplied by the best fit estimation of dithionite-reduced Δ*nifB*Δ*nifZ* MoFe protein magnetization curve has a value of 0.86 (Fig. 10). The magnetization contribution of dithionite-reduced Δ*nifH* MoFe protein at 520 nm is representative of the P^+ state of the latent P-cluster. The P^+ state of the P-cluster is paramagnetic with an $S = ½$ spin state. The paramagnetic

contribution of the S = ½ spin state contributes less to the magnetization curve of dithionite-reduced Δ*nifB*Δ*nifZ* MoFe protein.

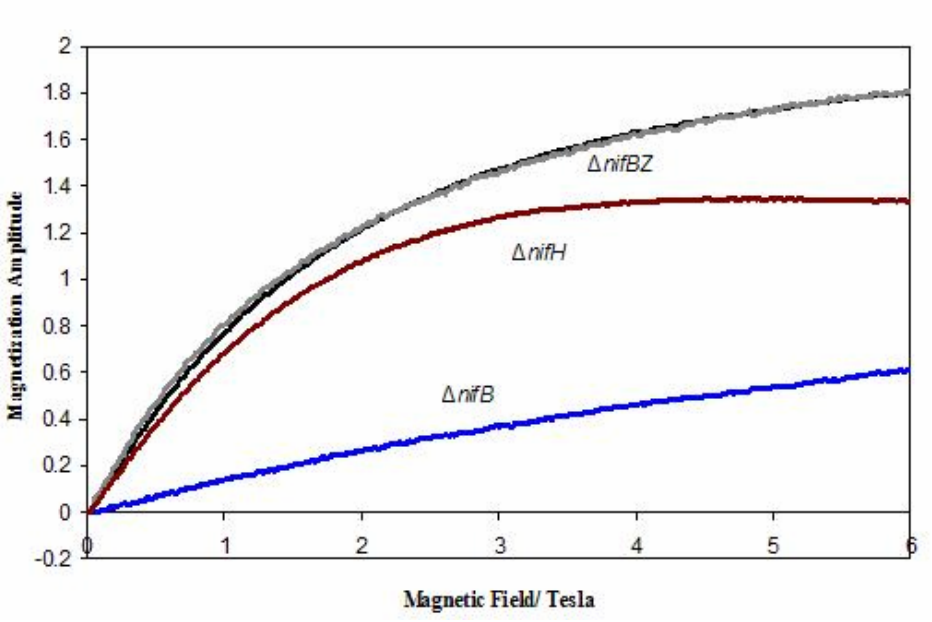

Fig. 10. Experimental magnetization curves of as-isolated MoFe proteins. Δ*nifB* MoFe protein, as-isolated Δ*nifH* MoFe protein, and as-isolated Δ*nifB*Δ*nifZ* MoFe protein. Simulation of factored magnetization curve contributions (gray curve) of as-isolated Δ*nifB* MoFe protein (blue curve) and as-isolated Δ*nifH* MoFe protein (red curve) shows a 1:1 ratio.

Figure 10 shows a simulation of factored contributions from the magnetization curves at 520 nm of the as-isolated, dithionite-reduced Δ*nifB* MoFe protein and the as-isolated, dithionite-reduced Δ*nifH* MoFe protein in an approximate 1:1 ratio is comparative to the experimental magnetization curve of the as-isolated, dithionite-reduced Δ*nifB*Δ*nifZ* MoFe protein. Based on comparative factoring the as-isolated dithionite reduced Δ*nifB*Δ*nifZ* MoFe protein has approximately a 1:1 ratio of as-isolated dithionite-reduced Δ*nifH* MoFe protein and Δ*nifB* MoFe protein.

SUMMARY AND CONCLUSIONS

Dithionite-reduced Δ*nifH* MoFe protein VT-MCD spectra is characteristic of an $S = ½$ $[4Fe\text{-}4S]^{+}$ cluster. The magnetization curve of dithionite-reduced Δ*nifH* MoFe protein lies relatively on a theoretically-simulated isotropic $g = 2$, $S = ½$ spin system magnetization curve. These studies are in agreement with the EPR spectroscopic studies and XAS that suggest dithionite-reduced Δ*nifH* MoFe protein an $S = ½$ spin system and [4Fe-4S]-like clusters, respectively.

The only difference in the low-temperature MCD spectra of dithionite-reduced Δ*nifB*Δ*nifZ* MoFe protein and Δ*nifH* MoFe protein is the intensity of the bands. This suggests the S =1/2 $[4Fe\text{-}4S]^{+}$ clusters observed in the low-temperature MCD spectra Δ*nifB*Δ*nifZ* MoFe protein are analogous to the same species revealed in the low-temperature MCD spectra of dithionite-reduced Δ*nifH* MoFe protein. The magnetization curve of dithionite-reduced Δ*nifB*Δ*nifZ* MoFe protein shows the possible presence of a diamagnetic component attributable to a fully-assembled P-cluster in its P^{N} state.

VT-MCD spectroscopy and magnetization studies show the multiple clusters of dithionite-reduced Δ*nifB*Δ*nifZ* MoFe protein have a 1:1 ratio of the clusters known to be in dithionite-reduced Δ*nifH* MoFe protein and dithionite-reduced Δ*nifB* MoFe protein. This is in agreement with previous EPR spectroscopic analysis that suggests the presence of two different cluster species in dithionite-reduced Δ*nifB*Δ*nifZ* MoFe protein, one being a normal P cluster (P^{N}) as found in dithionite-reduced Δ*nifB* MoFe protein and wild-type MoFe protein. The other cluster, through analysis of VT-MCD spectroscopy shows remarkable similarities to the P-cluster (P^{+}) precursors found in dithionite-reduced Δ*nifH* MoFe protein.

Magnetization curves of dithionite-reduced Δ*nifB*, Δ*nifH*, and Δ*nifB*Δ*nifZ* MoFe protein were analyzed to find the magnetization contribution of dithionite-reduced Δ*nifB* MoFe protein and Δ*nifH* MoFe protein to that of dithionite-reduced Δ*nifB*Δ*nifZ* MoFe protein. These studies indicate the amount of fully-assembled P-cluster and that of a latent or P-cluster precursor are in a 1:1 ratio in Δ*nifB*Δ*nifZ* MoFe protein.

This study provides a sound basis for assigning cluster type and oxidation state of the metallo-clusters found in dithionite-reduced Δ*nifB*Δ*nifZ* MoFe protein. The low-temperature MCD spectrum has a band pattern characteristic of a $[4Fe\text{-}4S]^{+}$ cluster. The magnetization studies at the absorption maxima revealed the ground state properties of an S = ½ spin system with contributions from a diamagnetic species.

Since there are 16 iron atoms present in dithionite-reduced Δ*nifB*Δ*nifZ* MoFe protein and 8 are assigned to a fully assembled P-cluster, then the [4Fe-4S] characteristic MCD spectra are related to 2-[4Fe-4S] P-cluster precursors. This study characterizes the as-isolated Δ*nifB*Δ*nifZ* MoFe protein to contain a fully assembled P-cluster ([8Fe-7S]) in one αβ subunit and a latent P-cluster (2-[4Fe-4S] clusters) in the other αβ subunit.

REFERENCES

1. Nitrogen Fixation at the Millennium. G. Jeffery Leigh, Editor. Elsevier Science

2. The fundamentals of nitrogen fixation. J. R. Postgate, FRS. Cambridge University Press.

3. Nitrogen Fixation in Bacteria and Higher Plants. R. C. Burns and R. W. F. Hardy. Spinger-Verlag Berlin. Heidelburg. New York 1975.

4. Howard, J. B. and D. C. Rees (1996). "Structural Basis of Biological Nitrogen Fixation." Chem. Rev. **96**, 2965-2982.

5. Hales, B. J., E. E. Case, J. E. Morningstar, M. F. Dzeda (1986). "Isolation of a new Vanadium-containing Nitrogenase from *A. vinelandii*." Biochemistry **25**, 7251-7255.

6. Georgiadis, M. M., H. Komiya, P. Chakrabarti, D. Woo, J. J. Kornuc, and D. C. Rees (1992). "Crystallographic Structure of the Nitrogenase Iron Protein from Azotobacter vinelandii." Science **257**, 1653-1659.

7. Kim, J. and D. C. Rees (1992). "Crystallographic structure and functional implications of the Nitrogenase molybdenum-iron protein from *Azotobacter vinelandii*." Nature **360**, 533-560.

8. Peters, J. W., M. H. B. Stowell, M. Solitis, M. G. Finnegan, M. K. Johnson, and D. C. Rees (1997). "Redox-Dependent Structrual Changes in the Nitrogenase P-cluster." Biochemistry **36** (6), 1181-1187.

9. Burgess, B. K. and D. J. Lowe (1996). "Mechanism of Molybdenum Nitrogenase." Chem. Rev. **96**, 2983-3011.

10. Lanzilotta, W. N., R. C. Holz, and L. C. Seefeldt (1995). "Proton NMR investigation of the $[4Fe\text{-}4S]^{1+}$ cluster environment of Nitrogenase iron protein from *Azotobacter vinelandii*: defining nucleotide-induced conformational changes." Biochemistry **34**, 15646-15653.

11. Einsle, O., D. Rees (2002). "Nitrogenase MoFe-Protein at 1.16 Resolution: A Central Ligand in the FeMo-cofactor." Science 297, 1696-1700.

12. Lindahl, P. A., E. P. Day, T. A. Kent, W. H. Orme-Johnson, and E. Munk (1985). "Mossbauer, EPR, and magnetization studies of the *Azotobacter vinelandii* Fe protein. Evidence for a $[4Fe\text{-}4S]^{1+}$ cluster with spin S=3/2." J. Biol. Chem. **260**, 11160-11173.

13. Angove, H. C., S. J. Yoo, B. K. Burgess, and E. Münck (1997). "Mossbauer and EPR Evidence for an all-Ferrous Fe_4S_4 Cluster with $S = 4$ in the Fe protein of Nitrogenase." J. Am. Chem. Soc. **119**, 8730-8731.

14. , H. C., S. J. Yoo, E. Münck, and B. K. Burgess (1998). "An All-ferrous State of the Fe Protein of Nitrogenase." J. of Biol. Chem. **273**, 26330-26337.

15. Peters, J. W., K. Fisher, W. E. Newton, D. R. Dean (1995). "Involvement of the P cluster in Intramolecular Electron Transfer within the Nitrogenase MoFe Protein." J. Biol. Chem. **270**, 27007-27013.

16. Lanzilotta, W. N. and L. C. Seefeldt (1996). "Electron Transfer from the Nitrogenase Iron Protein to the [8Fe-(7/8)S] Clusters of the Molybdenum-iron Protein." Biochemistry **35**, 16770-16776.

17. Lanzilotta, W. N., J. C, D. Dean, and L. Seefeldt (1999). "Spectroscopic Evidence for Changes in the Redox State of the Nitrogenase P-cluster during Turnover." Biochemistry **38**, 5779-5785.

18. Lowe, D. J. and R. N. F. Thorneley (1984). "The Mechanism of *Klebsiella pneumonia* nitrogenase action. Pre-steady-state kinetics of H2 formation." J. Biochem. **224**, 877-886.

19. Lowe, D. J., K. Fisher, R. N. F. Lowe (1993). "Klebsiella pneumoniae Nitrogenase: Pre-Steady-State Absorbance Changes Show that Redox Changes Occur in the MoFe Protein that Depend on Substrate and Component Protein Ratio; a Role for P-Centres in Reducing dinitrogen?" Biochem. J. **292**, 93-98.

20. Christiansen, J., R. C. Tittsworth, B. J. Hales, and S. P. Cramer (1995). "Fe and Mo EXAFS of *Azotobacter vinelandii* Nitrogenase in Partially Oxidized and Singly Reduced Forms." J. Am. Chem. Soc. **117**, 10017-10024.

21. Hagen, W. R., H. Wassink, R. R. Eady, B. E. Smith, and H. Haaker (1987). "Quantitative EPR of an S = 7/2 system in thionine-oxidized MoFe protein of nitrogenase. A redefinition of the P-cluster concept." Eur. J. Biochem **169**, 457-465.

22. Surrerus, K. K., M. P. Hendrich, P. D. Christie, D. Rottgardt, W. H. Orme-Johnson, and E. Münck (1992). "Mossbauer and Integer-Spin EPR of the Oxidized P-Clusters of Nitrogenase: POX is a Non-Kramers System with a Nearly Degenerate Ground Doublet." J. Am. Chem. Soc. **114**, 8579-8590.

23. Tittsworth, R. and B. J. Hales (1993). "Detection of EPR Signals Assigned to the 1-equiv-Oxidized P-clusters of the Nitrogenase MoFe-Protein form *A. vinelandii*." J. of Am. Chem. Soc. **115**, 9703-9707.

24. Pierik, A. J., H. Wassink, H. Haaker, and W. R. Hagen (1993). "Redox properties and EPR spectroscopy of the P clusters of *Azotobacter vinelandii* MoFe protein." Eur. J. Biochem. **212**, 51-61.

25. Hu, Y., A. Fay, P. C. Dos Santos, F. Naderi, and M. Ribbe (2004). "Characterization of *Azotobacter vinelandii nifZ* Deletion Strains Indication of Stepwise MoFe Protein Assembly." J. Biol. Chem. 279, 54963-54971.

26. Dos Santos, P. C., D. R. Dean, Y. Hu, and M. W. Ribbe (2004). "Formation and Insertion of the Nitrogenase Iron-Molybdenum Cofactor." Chem. Rev. **104**, 1159-1173.

27. Hu. Y., A. W. Fay, and M. W. Ribbe (2005). "Identification of a nitrogenase FeMo cofactor precursor on NIFEN complex." PNAS. **102**, 3236-3241.

28. Rubio, L. M. and P. W. Ludden (2005). "Maturation of Nitrogenase: a Biochemical Puzzle." J. of Bacteriology **187**, 405-414.

29. Blanchard, C. Z. and B. J. Hales (1996). "Isolation of Two Forms of the Nitrogenase VFe Protein from *Azotobacter vinelandii*." Biochemistry **35**, 472-478.

30. Roat-Malone (2002). Bioinorganic Chemistry A Short Course. Hoboken, John Wiley & Sons, Inc.

31. Ludden, P. W., V. K. Shah, J. R. Allen, and N. J.Spangler (1994). "In Vitro Synthesis of the Iron-Molybdenum Cofactor of Nitrogenase, Purification and Characterization of NifB Cofactor, The Product of NifB Protein." J. Biol. Chem. **269** (2), 1154-1158.

32. Christiansen, J., P. J. Goodwin, W. N. Lanzilotta, L. C. Seefeldt, and D. R. Dean (1998). "Catalytic and Biophysical Properties of a Nitrogenase Apo-MoFe protein Produced by a *nifB*-Deletion Mutant of *Azotobacter vinelandii*." Biochemistry **37**, 12611-12623.

33. Ribbe, M. W., Y. Hu, M. Guo, B. Schimdt, and B. K. Burgess (2002). "The FeMo-deficient MoFe Protein Produced by a *nifH* Deletion Strain of *Azotobacter vinelandii* Shows Unusual P-cluster Features." J. Biol. Chem. **277** (26), 23469-23476.

34. Broach, R., K. Rupnik, Y. Hu, A. W. Fay, and J. Webber, M. Cotton, M. W. Ribbe, and B. Hales. "VTVH-MCD Spectroscopic Study of the Metal Clusters in the Δ*nifB* and Δ*nifH* MoFe Proteins from *Azotobacter vinelandii*" Biochemistry. (accepted, in print).

35. Corbett, M. C., Y. Hu, F. Naderi, M. W. Ribbe, B. Hedman, and K. O. Hodgson (2004). "Comparison of Iron-Molybdenum Cofactor-deficient Nitrogenase MoFe Proteins by X-ray Absorption Spectroscopy. Implications for P-cluster Biosynthesis." J. Biol. Chem. **279** (27), 28276-28282.

36. Tal, S., T. W. Chun, M. Gavin, and B. K. Burgess (1991). "The Δ*nifB* (or Δ*nifE*) FeMo Cofactor-Deficient MoFe Protein is Different from the Δ*nifH* Protein." J. Biol. Chem. **266**, 10654-10657.

37. Schimdt, B. M. W. Ribbe, D. Rees (2002). "Structure of a cofactor-deficient Nitrogenase MoFe Protein." Science **296**, 352-356.

38. Burgess, B. K., D. B. Jacobs, and E. I. Stiefel (1980). "Large-Scale Purification of High Activity *Azotobacter vinelandii* Nitrogenase." Biochimica et Biophysica Acta. **614**, 196-209.

39. Stephens, P. J., A. J. Thomson, T. A. Keiderling, J. Rawlings, K. K. Rao, and D. O. Hall (1978). "Cluster characterization in iron-sulfur proteins by magnetic circular dichroism." Biochemistry **75**, 5273-5275.

40. Stephens, P. J., A. J. Thomson, J. B. R. Dunn, T. A. Keiderling, J. Rawlings, K. K. Rao, and D. O. Hall (1978). "Circular Dichroism and Magnetic Circular Dichroism of iron-Sulfur Proteins." Biochemistry **17**, 4770-4778.

41. Robinson, A. E., A. J. M. Richards, A. J. Thomson, T. R. Hawkes, and B. E. Smith (1984). "Low-temperature magnetic-circular-dichroism spectroscopy of the iron-molybdenum cofactor and the complementary cofactor-less MoFe protein of *Klebsiella pneumoniae* nitrogenase." J. Biochem. **219**, 495-503.

42. Neese, F. and E.I. Solomon (1999). "MCD C-Term Signs, Saturation Behavior, and Determination of Band Polarizatons in Randomly Oriented Systems with Spin $S \geq ½$. Applications to $S = ½$ and $S = 5/2$." Inorg. Chem. **38**, 1847-1865.

43. Zambrano, I. C., A. T. Kowal, L. E. Mortenson, M. W. W. Adams, and M. K. Johnson (1989). "Magnetic Circular Dichroism and Electron Paramagnetic Resonance Studies of Hydrogenases I and II from *Clostridium pasteurianum*." J. Biol. Chem. **264**, 20974-20983.

44. Stephens, P. J., C. E. McKenna, M. C. McKenna, H. T. Nguyen, and F. Devlin (1981). "Circular Dichroism and Magnetic Circular Dichroism of Reduced Molybdenum-Iron Protein of *Azotobacter vinelandii* Nitrogenase." Biochemistry **20**, 2857-2864.

45. Thomson, A. and M. K. Johnson (1980). "Magnetization curves of haemoproteins measured by low-temperature magnetic-circular-dichroism spectroscopy." J. Biochem. **191**, 411-420.

46. Morningstar, J. E., M. K. Johnson, E. E. Case, and B. J. Hales (1987). "Characterization of the Metal clusters in the Nitrogenase Molybdenum-Iron and Vanadium-Iron Proteins of *Azotobacter vinelandii* Using Magnetic circular Dichroism Spectroscopy." Biochemistry **26**, 1795-1800.

47. Christiansen, J., P. J. Goodwin, W. N. Lanzilotta, L. C. Seefeldt, and D. R. Dean (1998) "Catalytic and Biophysical Properties of a Nitrogenase Apo-MoFe Protein Produced by a *nifB*-Deletion Mutant of *Azotobacter vinelandii*" Biochemistry **37**, 12611-12623.

48. Thomson, A. J., S. J. George, A. J. M. Richards, A. E. Robinson, H. J. Grande, C. Veeger, and C. Van Dijk (1985). "A Study of one of the iron-sulphur clusters in oxidized hydrogenase from *Megasphaera elsdenii* by magnetic-circular-dichroism spectroscopy." J. Biol. Chem. **227**, 333-336.

VITA

Marcia Cotton was born on the sixteenth day of September in the year of nineteen hundred seventy-three. She is the fourth of seven daughters born to Henry Charles and Inez Cotton. Marcia was born and raised in the city of Bastrop, Louisiana. After graduating from Bastrop High School in nineteen hundred ninety-one, Marcia began her undergraduate studies at Mississippi University for Women in Columbus, Mississippi. She became a member of Delta Sigma Theta Sorority Incorporated via the Omicron Epsilon Chapter in nineteen hundred ninety-three. Marcia pursued a degree in Chemistry and received her Bachelor of Science in May of nineteen hundred ninety-five. Marcia started a career in teaching before beginning graduate studies at Louisiana State University in Baton Rouge, Louisiana. Her graduate work was performed in the laboratory of Professor Brian J. Hales.